Journal of Nano- and Electronic Physics
Vol. **12** No 6, 06032(5pp) (2020)

Журнал нано- та електронної фізики
Том **12** № 6, 06032(5cc) (2020)

Optical Properties of $Hg_{1-x}Mn_xS$, $Hg_{1-x-y}Mn_xFe_yS$, $Hg_{1-x-y}Mn_xFe_ySe_{1-z}S_z$

G.O. Andrushchak*, P.D. Maryanchuk

Yuriy Fedkovych Chernivtsi National University, 2, Kotsyubynsky St., 58012 Chernivtsi, Ukraine

(Received 12 June 2020; revised manuscript received 19 December 2020; published online 25 December 2020)

In this paper, the optical properties of $Hg_{1-x}Mn_xS$, $Hg_{1-x-y}Mn_xFe_yS$, $Hg_{1-x-y}Mn_xFe_ySe_{1-z}S_z$ crystals were studied. $Hg_{1-x}Mn_xS$, $Hg_{1-x-y}Mn_xFe_yS$, $Hg_{1-x-y}Mn_xFe_ySe_{1-z}S_z$ semimagnetic semiconductor solid solutions (their area of existence is $0 < x \leq 0.375$) obtained by the Bridgman method have n-type conductivity (electron concentration is $n \sim 10^{18}$ cm^{-3}). $Hg_{1-x}Mn_xS$, $Hg_{1-x-y}Mn_xFe_yS$, $Hg_{1-x-y}Mn_xFe_ySe_{1-z}S_z$ solid solutions are semiconductors with variable bandwidth dependent on the composition (E_g) and belong to semimagnetic semiconductors. The presence of Mn atoms in the crystals with an uncompensated magnetic moment makes it possible to control the composition (x).The refractive index and effective mass of electrons at the Fermi level for $Hg_{1-x}Mn_xS$, $Hg_{1-x-y}Mn_xFe_yS$ were determined on the basis of studies of the reflection coefficient. The transmission spectra were investigated at room temperature ($T \sim 300$ K). The optical band gap width of semiconductors under study was determined and the dominant mechanisms of electron scattering were established. It was found out that direct interband optical transitions take place in the studied crystals.

Keywords: Semiconductor, Mercury chalcogenides, Effective mass, Refractive index, Optical band gap.

DOI: 10.21272/jnep.12(6).06032 PACS numbers: 73.61.Le, 81.40.Tv

1. INTRODUCTION

Solid solutions on the basis of $A^{II}B^{VI}$ containing 3*d* elements belong to semimagnetic semiconductors. The currently known results of scientific research show that there is great interest in this group of solids [1].

One of the important features of semiconductors is the dependence of their physical properties on lighting (exposure to electromagnetic radiation of visible and infrared spectral regions). Under the influence of light, a number of physical effects is produced in semiconductors (e.g. the change in electrical conductance, the occurrence of electromotive forces, etc.), which constitute the work basis of a wide class of semiconductor devices: photodiodes, phototriodes, photodetectors, photoluminescence devices, solar cells, etc.

Solid solutions based on mercury chalcogenides are of particular interest for research in electronics. These solutions may contain such components as wide-bandgap or zero-gap diamagnetic semiconductors, e.g. HgS, HgSe [2-4] or MnS, FeS – wide-bandgap anti- or ferromagnetics [5].

The efficiency of operation of semiconductor photoelectric devices is determined by the processes that take place in semiconductors under light and, in turn, depend on a number of factors: purity and perfection of the crystal structure of semiconductor material, photon energy and radiation intensity, temperature, external fields (electric, magnetic), etc.

The change of structure leads to a gradual rearrangement of the energy band structure of these solid solutions. The presence of the magnetic component (Mn, Fe) in semimagnetic semiconductors causes different types of exchange interaction [6], which affects the band parameters of crystals and changes with the content of the magnetic component and under the influence of a magnetic field, temperature and heat treatment in the pairs of components [7].

2. RESULTS OF RESEARCH

2.1 Optical Properties of $Hg_{1-x}Mn_xS$, $Hg_{1-x-y}Mn_xFe_yS$, $Hg_{1-x-y}Mn_xFe_ySe_{1-z}S_z$ Crystals

The concentration of electrons obtained from Hall coefficient measurements equals to $n \sim 10^{18}$ cm^{-3}. The samples for kinetic research were made from parts of the crystal adjacent to those from which the samples were made for optical research. The magnetic component content of the samples was determined by magnetic susceptibility studies.

Measurements of the optical coefficients (T, R) were performed on a spectrometer Nicolet 6700 (attachment Pike was used for measuring R) within the wavelength interval $\lambda = 0.9$-26.6 μm. The angle of incidence in the attachment Pike can be changed within 30-80° for measuring reflection. The analysis of the dependences of R on the angle of incidence (Fig. 1) of non-polarized radiation showed that within the incidence angle domain from 30° to 55° R slightly changes, and thus the following can be assumed: $R(0°) \div R(55°) \approx$ const.

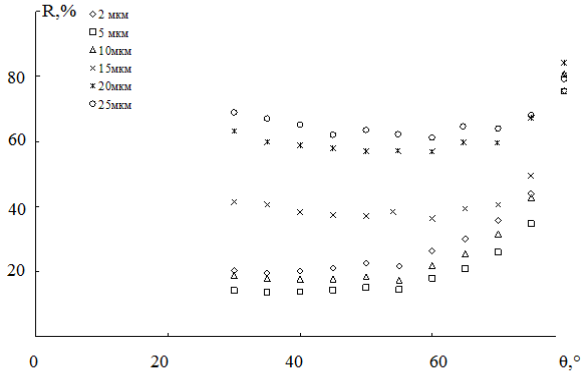

Fig. 1 – Dependence of R on the ray's angle of incidence for $Hg_{1-x}Mn_xS$ ($x_m = 0.03$) crystals (dependences are presented for different wavelengths, which are shown in the figure)

*g.andrushchak@chnu.edu.ua

At normal ray incidence, the connection between the reflection coefficient (R), refractive indexes (n) and absorption coefficients (k) is shown by the ratio [1]

$$R = \frac{(n-1)^2 + k^2}{(n+1)^2 - k^2}. \quad (1)$$

In real semiconductor crystals, the energy region, where absorption can be neglected, is in most cases small, but the condition $n^2 \gg k^2$ is fulfilled in a much larger region, so the refractive index was determined on the basis of the value of the reflection coefficient of non-polarized radiation (at an angle of incidence close to normal) by formula (2)

$$R = \frac{(n-1)^2}{(n+1)^2}, \quad (2)$$

which gave a sufficiently reliable value of the refractive index (n) in a wide range of photon energies (at least, for $\hbar\omega < E_g$).

On the basis of the dependences $R = f(\lambda)$ we determined the value of the refractive index for $Hg_{1-x}Mn_xS$ ($x_m = 0.03$) and $Hg_{1-x-y}Mn_xFe_yS$ ($x_m = 0.05$) solid solution crystals, which does not depend on the wavelength (Table 1).

Table 1 – The refractive index

Crystal	n
$Hg_{1-x}Mn_xS$ ($x_m = 0.03$)	2.55
$Hg_{1-x-y}Mn_xFe_yS$ ($x_m = 0.05$)	2.4

Electrons and holes form plasma in a semiconductor crystal. One of the properties of this plasma is its attempts to preserve the electrical neutrality in each point of the crystal. If this neutrality is affected by electromagnetic radiation, the charged particles will start to oscillate at some specific plasma frequency (ω). Own plasma oscillations lead to the absorption of electromagnetic radiation, independent of the scattering mechanism of free charge carriers. This is clearly shown in the reduction of the reflection coefficient near the plasma frequency (plasma minimum) (Fig. 2).

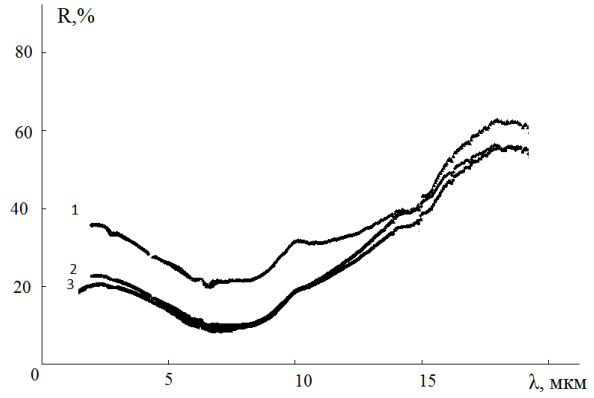

Fig.2 – Dependence of the reflection coefficient of $Hg_{1-x}Mn_xS$ ($x_m = 0.03$) samples on the wavelength of electromagnetic radiation at different angles of incidence: 1 – 30°, 2 – 50°, 3 – 70°

For all samples, with the increase in wavelength, the reflection coefficient decreases monotonically from 32 % to 10 %, passes through the minimum and increases sharply, reaching the values of ~ 70 %. The value of the effective mass of the electron at the Fermi level (m_ξ^*) can also be calculated from the condition of minimum:

$$m_\xi^* = \frac{e^2 N \lambda_{\min}^2}{\pi c^2 \left(\varepsilon_\infty - n_{\min}^2\right)}. \quad (3)$$

Since $R_{\min}$ is not too small ($R_{\min} \approx$ 9-20 % in the case of $Hg_{1-x}Mn_xS$), it is necessary to correct the ratio, so that the expression for the effective mass in the MKSA system, $\varepsilon_0 = 8.85 \times 10^{-12}$ F/m, will be the following:

$$m_\xi^* = \frac{e^2 N}{4\pi^2 c^2 \varepsilon_0} \times \frac{\lambda_{\min}^2}{\varepsilon_\infty - 1 + 4R_{\min}}. \quad (4)$$

According to this formula, we determined the value of the effective mass of electrons at the Fermi level (see Table 2).

Table 2 – The effective mass of electrons at the Fermi level

Crystal	n, cm^{-3}	$\lambda_{\min}$, μm	$R_{\min}$, %	m_ξ^*/m_0
$Hg_{1-x}Mn_xS$ ($x_m = 0.03$)	3×10^{18}	7.4	19	0.01
$Hg_{1-x-y}Mn_xFe_yS$ ($x_m = 0.05$)	1.2×10^{18}	8.2	22	0.01

Low values of the effective mass of electrons at the Fermi level are explained by the fact that the structure of $Hg_{1-x}Mn_xS$ ($x_m = 0.03$) and $Hg_{1-x-y}Mn_xFe_yS$ ($x_m = 0.05$) solid solutions is near zero-gap semiconductor/normal semiconductor transition (ZGS-NS). The obtained results of transmission coefficient measurements based on the wavelength of incident electromagnetic radiation for $Hg_{1-x-y}Mn_xFe_yS$ crystals are presented in Fig. 3, Fig. 4; for $Hg_{1-x}Mn_xS$, $Hg_{1-x-y}Mn_xFe_ySe_{1-z}S_z$ crystals dependences are similar.

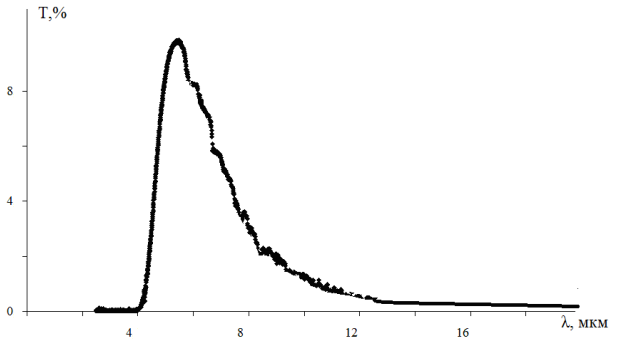

Fig. 3 – The dependence of the transmission coefficient on the wavelength of electromagnetic radiation for $Hg_{1-x-y}Mn_xFe_yS$ ($x_m = 0.05$) at $T \approx 300$ K, $d = 440$ μm

Fig. 4 shows that for $Hg_{1-x-y}Mn_xFe_yS$ ($x_m = 0.12$) crystals in the region of $\lambda \approx 5$ μm at energies of light quanta less than E_g, we can observe an additional absorption band, which is not connected with the transitions of the level-zone type – electrons do not transfer to the conduction band, but from the ground to the excited Fe^{2+} ion level. This band has a typical form, which is characteristic of crystals with an admixture of 3d elements in semiconductors of II-VI type [1, 8].

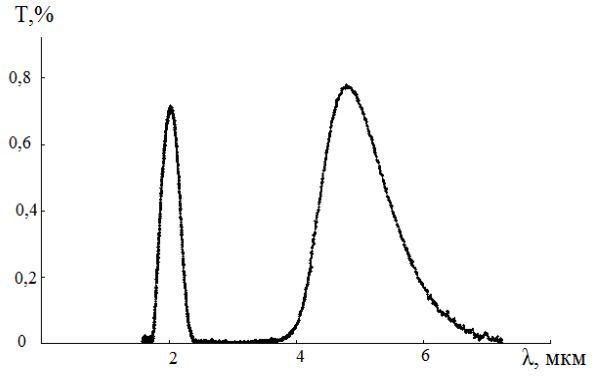

Fig. 4 – The dependence of the transmission coefficient on the wavelength of electromagnetic radiation for $Hg_{1-x-y}Mn_xFe_yS$ ($x_m = 0.12$) at $T \approx 300$ K, $d = 300$ μm

The observed absorption reflects the intracentral transitions between the levels of one Fe^{2+} center without changing its charge state.

Crystals containing iron can be used for the production of a dual-split filter.

Transmission spectra were recalculated in the spectral dependence of the absorption coefficient $\alpha = f(\lambda)$ by formula (5) (at transmission coefficients t_1 and $t_2 < 10$ %)

$$\alpha = \frac{1}{d_2 - d_1} \ln \frac{I_1}{I_2}, \qquad (5)$$

where I_2 and I_1 are the intensities of the light beam that passed through the sample with thicknesses d_2 and d_1 (after regrinding and refiguring), respectively; or according to formula (2) (with a reflection coefficient $R \sim 30$ % in the region of transparency variation from $(1 - R)/(1 + R)$ to 10 %) [9]

$$\alpha = \frac{1}{d} \ln \left[\frac{(1-R)^2}{2t} + \sqrt{\frac{(1-R)^4}{4t^2} + R^2} \right], \qquad (6)$$

The dependences $\alpha = f(h\nu)$ were recalculated by formula (2) depending on $\alpha^2 = f(h\nu)$. There is a straight-line segment on the dependences $\alpha^2 = f(h\nu)$, which indicates that the direct allowed interband optical transitions can be found in the $Hg_{1-x}Mn_xS$, $Hg_{1-x-y}Mn_xFe_yS$, $Hg_{1-x-y}Mn_xFe_ySe_{1-z}S_z$ crystals at $T \approx 300$ K (see Fig. 5, Fig. 6). The extrapolation of straight-line segments of the dependences $\alpha^2 = f(h\nu)$ to $\alpha^2 = 0$ determined the value of the optical band gap (E_g^{on}) at $T = 300$ K. The results are presented in Table 3.

Table 3 – Band gap width of the mercury chalcogenide-based solid solutions

Solid solutions	x_m	$n \times 10^{-18}$, cm^{-3}	E_g^{on}, eV
$Hg_{1-x}Mn_xS$	0.06	0.5	0.25
$Hg_{1-x}Mn_xS$	0.03	3	0.18
$Hg_{1-x}Mn_xS$	0.18	–	0.72
$Hg_{1-x-y}Mn_xFe_yS$	0.05	2.3	0.27
$Hg_{1-x-y}Mn_xFe_yS$	0.06	2	0.25
$Hg_{1-x-y}Mn_xFe_yS$	0.12	–	0.65
$Hg_{1-x-y}Mn_xFe_ySe_{1-z}S_z$	0.03	6	0.32

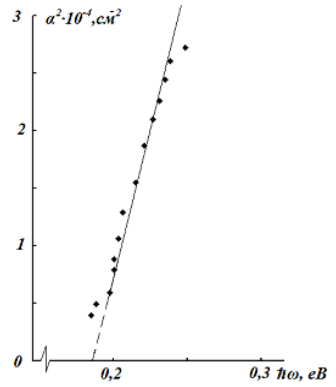

Fig. 5 – The α^2-dependence on the energy of incident electromagnetic radiation at $T \approx 300$ K for $Hg_{1-x}Mn_xS$ ($x_m = 0.03$, $n \sim 3 \times 10^{18}$ cm^{-3})

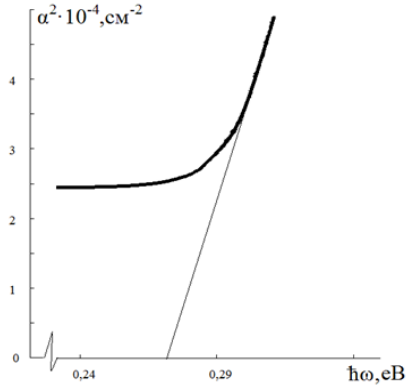

Fig. 6 – The α^2-dependence on the energy of incident electromagnetic radiation at $T \approx 300$ K for $Hg_{1-x-y}Mn_xFe_yS$ ($x_m = 0.05$, $n \sim 2.3 \times 10^{18}$ cm^{-3})

2.2 The Mechanisms of Electron Scattering in $Hg_{1-x}Mn_xS$, $Hg_{1-x-y}Mn_xFe_yS$ and $Hg_{1-x-y}Mn_xFe_ySe_{1-z}S_z$ Crystals

The dependences $\lg\alpha = f(\lg\lambda)$ were obtained on the basis of the dependences $\alpha = f(\lambda)$ (Fig. 7).

The slope of the long-wave region of $\lg\alpha = f(\lg\lambda)$ dependence, stipulated by absorption of electromagnetic waves by free charge carriers, was used to determine the exponent (r), which characterizes the dominant scattering mechanisms.

The classical theory based on the Drude-Lorentz model of an ideal electron gas provides a formula for the optical absorption coefficient of free charge carriers in the form of [10]

$$\alpha(\lambda) = \frac{Ne^2\lambda^2}{m^* 8\pi^2 nc^3 \tau(k)} \qquad (7)$$

where N is the carrier concentration, λ is the wavelength of absorbed photons, m^* is the effective mass of charge carriers, n is the light refractive index inside the crystal, c is the speed of light, $\tau(k)$ is the carrier relaxation time determined by the operating scattering mechanisms. According to this formula, absorption by free charge carriers grows as a square of the wavelength of absorbed photons, which corresponds to the inversely proportional dependence on the square of the

frequency. A more precise quantum-mechanical account of specific scattering mechanisms causes these dependences of the absorption coefficient by free charge carriers on the wavelength of absorbed photons:

$\alpha(\lambda) \sim \lambda^{3/2}$ – for scattering by acoustic phonons;

$\alpha(\lambda) \sim \lambda^{5/2}$ – for scattering by optical phonons;

$\alpha(\lambda) \sim \lambda^{3}$ or $\lambda^{/2}$ during scattering by ion admixtures.

In general, all scattering mechanisms are performed and the absorption coefficient is the following sum:

$$\alpha(\lambda) = \sum \alpha_i(\lambda) = C_1\lambda^{3/2} + C_2\lambda^{5/2} + C_3\lambda^{7/2}. \quad (8)$$

Depending on the concentration of admixtures, temperature and predominant type of lattice oscillations, this or that scattering mechanism will dominate.

The slope of the long-wave region of $\lg\alpha = f(\lg\lambda)$ dependence (Fig. 7), stipulated by absorption of electromagnetic waves by free charge carrier as $\lg\alpha \sim r\lg\lambda$ and $r \sim \lg\alpha/\lg\lambda$, was used to determine the exponent (r), which characterizes the dominant scattering mechanisms ($r = 1.5$ for scattering by acoustic phonons, $r = 2.5$ – by optical phonons, $r = 3$-3.5 – by ion admixtures).

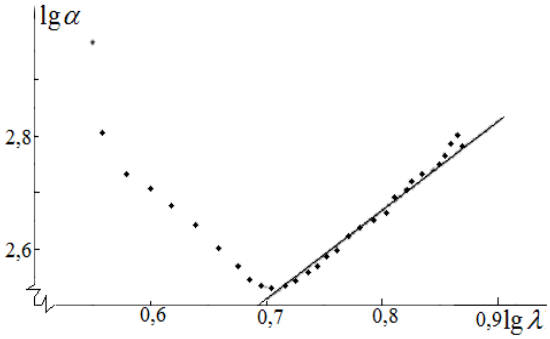

Fig. 7 – Dependence of $\lg\alpha$ on $\lg\lambda$ for $Hg_{1-x-y}Mn_xFe_ySe_{1-z}S_z$ ($x_m = 0.03$; $z = 0.01$), where α [cm^{-1}], λ [μm], $T \approx 300$ K

The value of the r-parameter for the investigated $Hg_{1-x-y}Mn_xFe_ySe_{1-z}S_z$ solid solutions is $r = 1.9$, which corresponds to the dominance of combined electron scattering by acoustic and polar optical phonons (by the mentioned phonons at $T > \theta_d$, $\theta_d \sim 225$ K).

For the $Hg_{1-x}Mn_xS$ ($x = 0.06$) crystals $r = 2.2$, for $Hg_{1-x-y}Mn_xFe_yS$ ($x = 0.06$) – $r = 2.5$, which corresponds to the dominance of electron scattering by polar optical phonons. These results are in accordance with the results obtained on the basis of studies of kinetic coefficients.

It should be noted that the composition (x) and concentration of electrons (n) in the samples under study (for optical properties) are equal to those values that were obtained from the measurements of magnetic susceptibility and Hall effect for the samples cut from the adjacent bead.

3. CONCLUSIONS

1. On the basis of the dependences $R = f(\lambda)$ the value of the refractive index for the $Hg_{1-x}Mn_xS$ ($x_m = 0.03$) and $Hg_{1-x-y}Mn_xFe_yS$ ($x_m = 0.05$) solid solution crystals was calculated.

2. On the basis of the study of the reflection and transmission coefficients, the $\alpha^2 = f(h\nu)$ dependences were obtained, where we can observe the straight-line segments indicating that the studied crystals contain direct allowed interband optical transitions.

3. The extrapolation of straight-line segments of the $\alpha^2 = f(h\nu)$ to $\alpha^2 = 0$ determined the value of the optical band gap (E_g^{on}).

4. The slope of the long-wave region of $\lg\alpha = f(\lg\lambda)$ dependence was used to determine the parameter r ($2 < r \leq 2.5$) of the studied crystals, which corresponds (at $T > \theta_d$) to the dominance of electron scattering by polar optical phonons.

REFERENCES

1. I.P. Koziarskyi, P.D. Marianchuk, E.V. Maistruk, *Ukr. J. Phys. Opt.* **12**, 137 (2011).
2. N.M. Hosny, A. Dahshan, *J. Mol. Struct.* **1085**, 78 (2015).
3. B. Patel, S. Rath, S. Sarangi, S.N. Sahu, *Appl. Phys. A* **86**, 447 (2007).
4. M. Esmaeili-Zare, M. Salavati-Niasari, *Res. Chem. Intermed* **41**, 8185 (2015).
5. A.N. Utyuzh, *Phys. Solid State* **56**, 2050 (2014).
6. X. Li, J. Cao, L. Yang, M. Wei, X. Liu, Q. Liu, J. Du, J. Wang, Y. Zhou, J. Yang, *Appl. Phys. A* **124**, 671 (2018).
7. V.A. Sidorov, J. Guo, L. Sun, V.V. Brazhkin, *JETP Lett.* **107**, 311 (2018).
8. I.P. Koziarskyi, E.V. Maistruk, D.P. Koziarskyi, *Proc. SPIE.* **9066**, 90661E (2013).
9. T.T. Kovalyuk, P.D. Maryanchuk, E.V. Maistruk, I.P. Koziarskyi, *Inorg. Mater.* **50**, 241 (2014).
10. P.D. Maryanchuk, I.P. Koziarskyi, *Inorg. Mater.* **48**, 655 (2012).

Оптичні властивості $Hg_{1-x}Mn_xS$, $Hg_{1-x-y}Mn_xFe_yS$, $Hg_{1-x-y}Mn_xFe_ySe_{1-z}S_z$

Г.О. Андрущак, П.Д. Мар'янчук

Чернівецький національний університет імені Юрія Федьковича, вул. Коцюбинського 2, 58012 Чернівці, Україна

В роботі проведено дослідження оптичних властивостей кристалів $Hg_{1-x}Mn_xS$, $Hg_{1-x-y}Mn_xFe_yS$, $Hg_{1-x-y}Mn_xFe_ySe_{1-z}S_z$. Напівмагнітні напівпровідникові тверді розчини $Hg_{1-x}Mn_xS$, $Hg_{1-x-y}Mn_xFe_yS$, $Hg_{1-x-y}Mn_xFe_ySe_{1-z}S_z$ (область існування яких $0 < x \leq 0{,}375$), одержані методом Бріджмена, володіють провідністю n-типу (концентрація електронів $n \sim 10^{18}$см$^{-3}$). Тверді розчини $Hg_{1-x}Mn_xS$, $Hg_{1-x-y}Mn_xFe_yS$ та $Hg_{1-x-y}Mn_xFe_ySe_{1-z}S_z$ є напівпровідниками із змінною в залежності від складу шириною забороненої зони (E_g) і належать до напівмагнітних напівпровідників. Наявність в кристалах атомів Mn із нескомпенсованим магнітним моментом дає можливість контролювати склад (x). На основі досліджень

коефіцієнту відбивання визначені показники заломлення і ефективна маса електронів на рівні Фермі для $Hg_{1-x}Mn_xS$, $Hg_{1-x-y}Mn_xFe_yS$. Дослідження спектрів пропускання проведено при кімнатній температурі $T \sim 300$ K. Визначена оптична ширина забороненої зони досліджуваних напівпровідників і встановлені домінуючі механізми розсіювання електронів. Показано, що в досліджуваних кристалах наявні прямі міжзонні оптичні переходи.

Ключові слова: Напівпровідник, Халькогеніди ртуті, Ефективна маса, Показник заломлення, Оптична ширина забороненої зони.